MoS2 nanoparticles decorating titanate-nanotube surfaces: Combined microscopy, spectroscopy, and catalytic studies

UNIVERSITÀ DEGLI STUDI DI TORINO

Langmuir, Volume 31, Issue 19, Pages 5469–5478; DOI: 10.1021/acs.langmuir.5b00396

MoS_2 Nanoparticles Decorating Titanate-Nanotube Surfaces: Combined Microscopy, Spectroscopy and Catalytic Studies

Sara Cravanzola[1], Lucia Muscuso[1], Federico Cesano[1], Giovanni Agostini[2], Alessandro Damin[1], Domenica Scarano[1] and Adriano Zecchina[1]*

[1]Dept. of Chemistry, NIS (Nanostructured Interfaces and Surfaces) Interdepartmental Centre and INSTM Centro Di Riferimento, University of Torino, Via P. Giuria, 7, 10125 Torino (Italy).

*Corresponding author: federico.cesano@unito.it

[2]Current address: giovanni.agostini@esrf.fr

KEYWORDS. MoS_2/TNTs; nanostructured hybrid composites; morphology, structure and optical properties; photocatalysis.

ABSTRACT. MoS_2/TNTs composites have been obtained by impregnation of titanate nanotubes (TNTs) with a centrifuged solution of nanosized MoS_2 particles in isopropyl alcohol (IPA). The characterization has been performed by combining UV-vis-NIR, Raman, AFM and HRTEM analyses, before and after impregnation. HRTEM images show that the contact between single layer MoS_2 nanoparticles and the support is efficient, so justifying the decoration concept. The volatility of IPA solvent allows the preparation of composites at low temperature and free of carbonaceous impurities. MoS_2 nanoparticles have strong excitonic transitions, which are only slightly shifted with respect to the bulk because of quantum size effects. Concentrations of MoS_2, less than 0.1 wt%, are enough to induce strong absorption in the visible. Photodegradation of methylene blue (MB) has been performed on TNTs and MoS_2/TNTs to verify the effect of the presence of MoS_2. The first layer of adsorbed MB is consumed first, followed by clustered MB in the second and more external layers. The presence of low concentrated MoS_2 nanoparticles does not substantially alter the photocatalytic properties of TNTs. This result is due to poor overlapping between the high frequency of MoS_2 C, D excitonic transitions and the TNTs band gap transition.

1. Introduction

After the discovery of graphene, a 2D material with excellent electronic conductivity, mechanical properties and high surface area, constituted by one atom-thick layer of carbon atoms packed with honeycomb lattice, studies on graphene applications and graphene-like materials have experienced a rapid growth.[1-3]

As far as carbon is concerned, by exploiting the high surface area, the associated improved interfacial contact potentialities and the optical properties, many carbon/TiO_2 composites have been recently obtained for use in lithium ion batteries,[4-5] photocatalysis,[6-10] and dye sensitized solar cells.[11-13]

Among the graphene-like materials, molybdenum disulphide (MoS_2), which is possessing the same layered structure of graphene and is composed by Mo atoms sandwiched between two layers of hexagonally closed-packed sulphur atoms, exhibits unique physical, optical and electrical properties correlated with its ultrathin and/or nanosized structure.[14-15] These properties are particularly important in several fields, like sensors, lithium batteries,[16] phototransistors,[15] photocatalysts, hydrogen production catalyst,[17-18] catalysts for hydrodesulfurization and hydrodenitrogenation processes.[19-20] To exploit the full potential of the molybdenum disulphide, it is often necessary to combine it with different kinds of materials like Au (111),[21]graphite,[22] and oxides (SiO_2, γ-Al_2O_3 and MgO).[23] The favourable optical properties of MoS_2 have been exploited to increase the visible light absorption ability of TiO_2. In fact TiO_2, although characterized by excellent photocatalytic properties, absorbs only a small portion of solar spectrum in the UV region (3% of the sunlight spectrum)[24] without absorption in the visible light interval.[14] To deal with such a problem, and then to improve the photocatalytic efficiency and functionality of TiO_2, the studies have focused on mixing active additives on a single-component photocatalysts[25] or on making heterogeneous semiconductor systems.[26]

Due to its absorption in the visible and UV range, MoS_2 was considered of great interest to perform hybrid materials, made by TiO_2 sensitized with exfoliated MoS_2.[27] Indeed MoS_2/TiO_2 composites showed high photocatalytic performance in the degradation of organic dyes.[25, 27-29] Recently some authors fabricated a solar cell based on MoS_2/TiO_2 hybrid nanocomposites.[28]

A difficulty encountered in the synthesis of MoS_2/TiO_2 composites is the tendency of TiO_2 particles to agglomerate thus causing a decrement of the adsorptive properties and a poor interfacial contact with the layered materials.[30] For this reason, peculiar TiO_2 morphologies providing a maximum interfacial contact without aggregation, have been explored.[31] TiO_2/nanoporous frameworks composites characterized by shape selective adsorption properties have also been proposed.[32]

Along this line, titanate nanotubes (TNTs), which can be considered as rolled 2-D nanostructures in form of nanotubes, are of interest. In fact they have a much higher surface area (inner and outer surface) and a higher number of active sites with respect to TiO_2, a fact which can favour the processes occurring on the surface, for instance the photocatalytic degradations of pollutants. Furthermore, due to their properties

(i.e., 1-D nanostructure, large surface-to-volume ratio, high ion-exchange),[33] layered systems can provide a better interfacial contact with supported phases, a fact which makes them suitable for the synthesis of composites. It is a matter of fact that increasing efforts have been focused on coupling TNTs with graphene[31, 34] or with other semiconductors (i.e. CdS).[33], but not with MoS_2. However, due to the quantum size effect associated with the 1D structure of TNTs, the band gap (~ 3.40 eV) is higher than that of TiO_2 (~ 3 eV), which is a 3D semiconductor. This fact is counterbalancing the potential positive aspects mentioned above mainly due to the much higher surface area associated with the 1D structure. Which of these aspects is predominating in determining the photocatalytic activity cannot be established *a priori*, even if the higher band gap of TNTs is expected to play a negative effect when photocatalysis is carried out using visible light.

As for MoS_2/TNTs composites is concerned, the favourable optical properties of MoS_2 (showing excitonic absorption bands in the visible) and the potentially good electrical contact between MoS_2 nanoparticles and titanate nanotubes (a fact, which can provide an efficient interfacial charge-transfer region), make this system potentially suitable for photocatalysis using visible light. It must be mentioned however that, due to the tendency of MoS_2 to form irregular aggregates of nanoparticles or stacked multilayers,[27] the deposition of MoS_2 nanostructures on substrates is difficult, a fact that can have negative effects on the interfacial contact. To overcome the aggregation problem and hence to maximize the contact between the TNTs and MoS_2 particles, in this work the preliminary exfoliation of MoS_2 has been performed by means of the solvent assisted ultrasonication. In fact, in a previous work we have known that an intense cavitation field, if carried out in a small volume with a relatively poor solvent (isopropyl alcohol), makes possible to exfoliate and to fragment thick flakes of stacked MoS_2 with the predominant formation of thin sheets and particles with lateral sizes comprised in the 3-15 nm interval and that the high dispersion is also favoured by the extensive surface functionalization, which is covering the edges with organic groups.[35] The fragmentation occurs via the great propagation of cracks perpendicularly to basal planes. After the ultracentrifugation, able to separate the nanoparticles from the thick flakes, the very diluted suspension containing MoS_2 nanoparticles can then be used to impregnate titanate nanotubes. The so obtained composite contains only a small amount of MoS_2 nanoparticles (lower than 0.1 wt.%). Despite the low MoS_2 content, the high intensity of the excitonic bands of supported MoS_2 nanoparticles makes the composite able to strongly absorb the visible light, a fact which could potentially induce the appearance of interesting photocatalytic properties. To verify whether the presence of diluted MoS_2 nanoparticles on TNTs surface characterized by excitonic absorption bands in the visible can alter the photocatalytic properties of TNTs, photodegradation experiments of methylene blue (MB) have been performed on TNTs and MoS_2/TNTs. The results have been compared with those obtained on pure TiO_2 (P25). In this paper we report results concerning the structure, the dispersion and the optical properties of the MoS_2 nanoparticles, both before and after deposition on TNTs, as studied by means of: atomic force microscopy (AFM), Raman spectroscopy, transmission electron microscopy

(TEM) and UV-vis-NIR spectroscopy. The photodegradation properties of TNTs and MoS_2/TNTs have also been investigated and compared with those of TiO_2 (P25).

2. Experimental

2.1 Exfoliation and fragmenting of MoS_2.

MoS_2 powders (2 mg, Aldrich) with an average particle size of ~ 6 μm, were dispersed in 10 mL isopropyl alcohol (IPA) and sonicated at 20 KHz for 12 hours by means of a VCX 500 Sonics Vibracell ultrasonic processor (power 500W), equipped with a Ti alloy tapered microtip (d= 3mm, 30% amplitude). A great intensity of cavitation can be obtained by the small diameter horn in the restricted volume of the solution, which has been placed in an ice bath to control the temperature during the whole sonication step. The obtained dark-gray and turbid solution was then centrifuged (30 minutes, 4000 rpm), thus allowing the sedimentation of bigger particles and the separation of a clear light green-yellow supernatant solution to occur. Only the top portion of the transparent ultracentrifuged solution has been collected and used for the subsequent impregnation step.

2.2 Synthesis of protonated titanate nanotube.

Protonated titanate nanotubes were obtained following the preparation procedure reported in [36]. Briefly, TiO_2 anatase (99.8%, Sigma Aldrich) was used as a precursor material, which was treated with a caustic solution (10 M NaOH) at 150°C for 18 hour placed in a PTFE autoclave to obtain sodium titanates. The obtained material was washed with distilled water and filtered several times (0.2 μm pore PC filter) for removing the exceeding reagents. Sodium titanates were then treated with HCl 0.1 M for 5 hours under stirring and then washed with distilled water several times and dried at 120°C to obtain protonated titanate nanotubes. The surface area, measured by the BET standard method was 300-350 m^2/g.

2.3 Synthesis of MoS_2/protonated titanate nanotube composites and measurement of vibrational and optical properties.

Increasing amounts of MoS_2 (coming from the supernatant and clear solution, which was obtained from the centrifugation of sonicated dispersion), were added to 0.1 g of protonated titanate nanotubes. After dropping aliquots of the MoS_2 solution (from 0.44 mL to 17.6 mL), a powdered material of increasing brownish colour was obtained (wet impregnation method). At the end of each step, the impregnated powder was dried at 100°C to remove the solvent. The final concentration of MoS_2 is not overcoming the 0.1 wt %. Higher MoS_2 concentrations have not been investigated because they are associated with too intense bands in the visible, a fact which precludes the accurate determination by reflectance spectroscopy of the optical properties of MoS_2 in interaction with TNTs.

2.4 Adsorption and degradation of methylene blue on TNTs, MoS_2/TNTs and TiO_2 (P25).

The powder samples, in form of pellets, (TNTs and MoS_2/TNTs, both 30 mg in weight) have been impregnated with 3 mL methylene blue (MB) water solution (25mg/l), then the solvent was eliminated by evaporation at room temperature under dark. By considering the specific surface area (SSA) of TNTs (~300-350 m^2/g)[36] and the sizes of MB (6.7 x 15.0 Å)[37], about 1.5 monolayers of MB were deposited on both systems. The same amount of MB was used to impregnate TiO_2 (P25) used as reference.

Photocatalytic degradation of adsorbed methylene blue (MB) on TNTs has been mainly investigated by reflectance spectroscopy. The simulating solar light irradiation was carried out at 25°C by using a SOL2/500S lamp (Honle UV technology, Munchen, Germany) for photocatalytic reactions. The SOL-bulb and the H_2 filter together yield a spectrum, which is very similar to the natural sunlight, ranging from ultraviolet to infrared radiation (approx 295–3000 nm).

The gradual disappearance of bands of MB adsorbed on the surface upon exposure to visible light for increasing times was also followed by reflectance spectroscopy. The integrated intensity of the adsorbed MB manifestations (I) was used to obtain the I/I_0 *vs.* time plots, where I_0 is the initial intensity before illumination. As for the integrated intensity of MB adsorbed on MoS_2/TNTs, it was obtained by subtracting the excitonic A- B bands of MoS_2 present in the background, which are not affected by the adsorption process.

To verify the correctness of the results obtained in reflectance mode, control photodegradation experiments were also performed by measuring the decrement of MB concentration in the solution in equilibrium with TNTs**,** MoS_2/TNTs and TiO_2 subjected to illumination for increasing time.

2.5 Characterization techniques.

The optical properties of sonicated MoS_2 and of the composite material were collected at room temperature by using UV-vis-NIR spectrophotometer (Varian Cary UV 5000) in the wavelength range of 190-2500 nm. The spectrum of sonicated and centrifuged MoS_2 solution was recorded in transmittance mode. The spectra of hybrid materials were recorded in diffuse reflectance mode by using the same instrument equipped with an integrating sphere.

The morphology of the particles contained in the sonicated and centrifuged solution and of MoS_2/TNTs composite powder has been obtained by means of:

i) atomic force microscopy with a Park Systems XE-100 in non-contact mode. The AFM images of the particles before impregnation of TNTs were obtained by depositing a few drops of the IPA solution on a mica substrate.

ii) transmission electron microscopy with a JEOL 3010-UHR instrument operating at 300 kV, equipped with a 2k×2k pixels Gatan US1000 CCD camera. The TEM images of particles before impregnation of TNTs were obtained by depositing a few drops of the sample onto a TEM grid and evaporating the solvent. Similarly TEM images of TNTs before and after impregnation were obtained on samples deposited on a carbon grid.

From HRTEM observations, a ML-MoS_2 model was constructed to simulate kinematic electron diffraction patterns and to identify the zone-axis direction and intersecting planes. Models, reciprocal lattice, simulated electron patterns and representations were obtained by means of CaRIne Crystallography 3.1 or by Diamond 3.0 software packages, respectively.

To fully characterize the composite, Raman spectra of bulk MoS_2, titanates nanotubes and MoS_2/TNTs composites were recorded at room temperature in air by using a Renishaw inVia Raman Microscope spectrometer equipped with an Ar^+ laser emitting at 442 nm. A 50X ''long working distance'' magnification objective has been adopted.

The photodegradation experiments of methylene blue (MB) on pure TNTs, MoS_2/TNTs hybrid system and TiO_2 (P25) have been performed in two ways. Following the first procedure the photodegradation of MB has been studied in the reflectance mode in the UV-vis range by measuring the gradual disappearance of the bands of adsorbed MB upon exposure to visible light for increasing time. The results of this experiment are reported in detail. Following the second procedure, after equilibration (a process, which as far as TNTs are concerned, takes very long time) the decrement with exposure time of MB concentration in the solution in equilibrium with the solid composite has been followed by means of UV-vis transmittance spectroscopy. This second procedure has been performed simply to confirm the correctness of the results of the first one. The results of the first procedure are highly informative because they are free from the uncertainties related to the equilibration; they give information not only on the reaction kinetics but also about the monomeric/polymeric species adsorbed on the surface and on their reactivity under visible light illumination.

3. Results and discussion

3.1. Morphology and structure of the sonicated MoS_2.

MoS_2 nanoparticles deposited on a grid from the upper fraction of sonicated and centrifuged solution, are TEM imaged in Figure 1. The choice of the upper fraction of the solution coming from the ultracentifugation is ensuring that the particle size is minimized. [35]

Besides the rare larger MoS_2 sheets, whose morphology will be better illustrated and discussed in the Figure 2, small slabs having size distributions with maxima in the 5-15 nm range are shown in Figure 1a. These results confirm that efficient exfoliation and fragmentation under sonication are both occurring, even in the "bad" isopropyl alcohol solvent, [35] which is not usually considered to be able to promote the stable formation of a population of mono- or few-layer MoS_2 nanosheets, like observed for N-Methyl-2-pyrrolidone, N-vinylpyrrolidinone, dimethylformamide or binary solvent-surfactant mistures having a surface tension of ~40 mJ/m^2 and suitable Hansen solubility parameters.[49] About the state of MoS_2 particles in the solution we shall return in the following when the UV-vis spectrum of the solution *(vide infra)* is commented.

TEM image (in Figure 1a) is mostly indicative of the particle size distribution. In many cases, aggregates of small particles deposited on flat MoS_2 slabs are also observed (see model in Figure 1a). It is

conceivable that these aggregates are the result of an aggregation process occurring during the solvent evaporation and that they are not present in the MoS_2 dispersion before IPA removal. More details on the structure of the particles can be obtained with high resolution transmission microscopy (Figure 1b). In particular, a MoS_2 nanosheet oriented along the [001] zone axis and exposing the basal plane is HRTEM imaged in Figure 1b.

The hexagonal MoS_2 structure is confirmed by the corresponding fast Fourier transform (FFT) imaged in Figure 1c, which shows bright spots 0.27 nm and 0.16 nm spaced and associated with {110} and {100} lattice fringes, respectively. The [001] zone axis for the MoS_2 slab is obtained by simulating the spatial orientation of a 2H-MoS_2 slab (Figure 1d and Supporting Information, Figure S1), whose reciprocal lattice has been used to obtain the experimental electron diffraction pattern (Figure 1c).

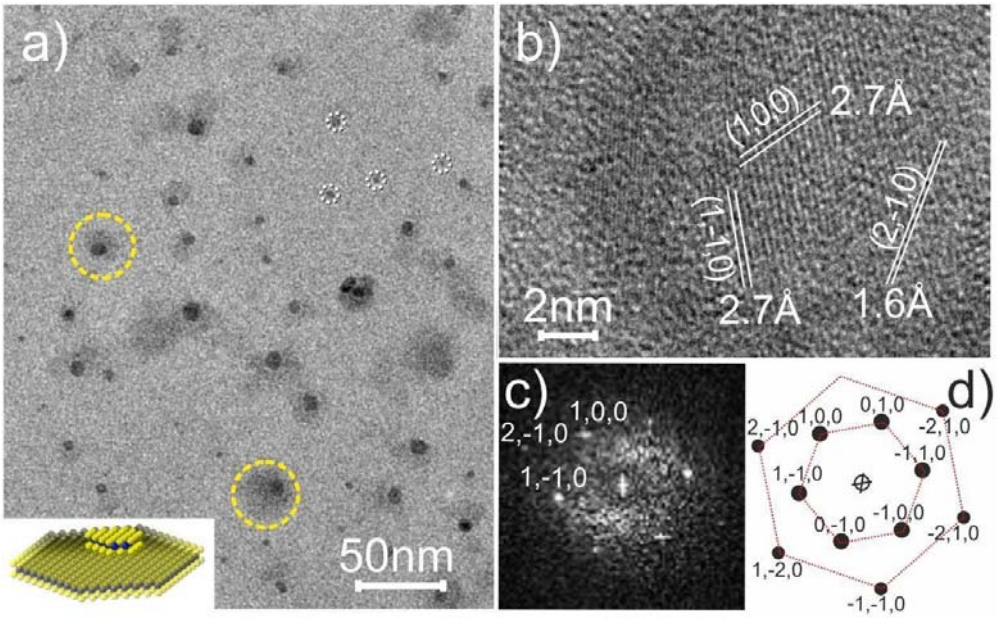

Figure 1. a) TEM images of the MoS_2 nanoparticles obtained from the sonication process. White dotted circles illustrate the smaller MoS_2 nanoparticles, yellow dashed circles illustrate aggregates formed by small particle deposited on the flat surface of a few layers slab; b) HRTEM images of a thin exfoliated MoS_2 nanoparticle exposing the basal-plane; c) experimental FFT image oriented along the [001] zone axis; d) simulated SAED pattern, as obtained from the experimental FFT image.

In Figure 2 the TEM image of a region containing partially exfoliated and fragmented particles, typically present in the medium of the ultrasonication cuvette, is illustrated. This image is giving information on the exfoliation/fragmentation process induced by sonication. Lattice fringes 0.65 nm spaced and corresponding to the (002) basal planes of MoS_2 nanosheets are observed. From this figure, the limited stacking effect ($1 \leq$ layers number ≤ 5) (arrows on the image and modelling on the left side of Figure 2), is further indicating that the exfoliation process, occurring in a relatively "bad solvent" like isopropyl alcohol,[35] is efficient. The effectiveness of the strong cavitation process is testified by defective regions, such as edge dislocations and plane curvatures (dotted circles on the image and modelling on the

right side of Figure 2), by the small lateral sizes of the slabs (few-nanometers large), which means that the slab fragmentation occurs perpendicularly to the basal planes *(vide infra).* Notice that, the few-layered MoS_2 looks flexible and sufficiently small in size to be arranged on irregular and curved surfaces or even to be potentially inserted into small pores. Whether the curvature is the result of the layers flexibility or of the presence of defects of atomic size cannot be inferred from the TEM images.

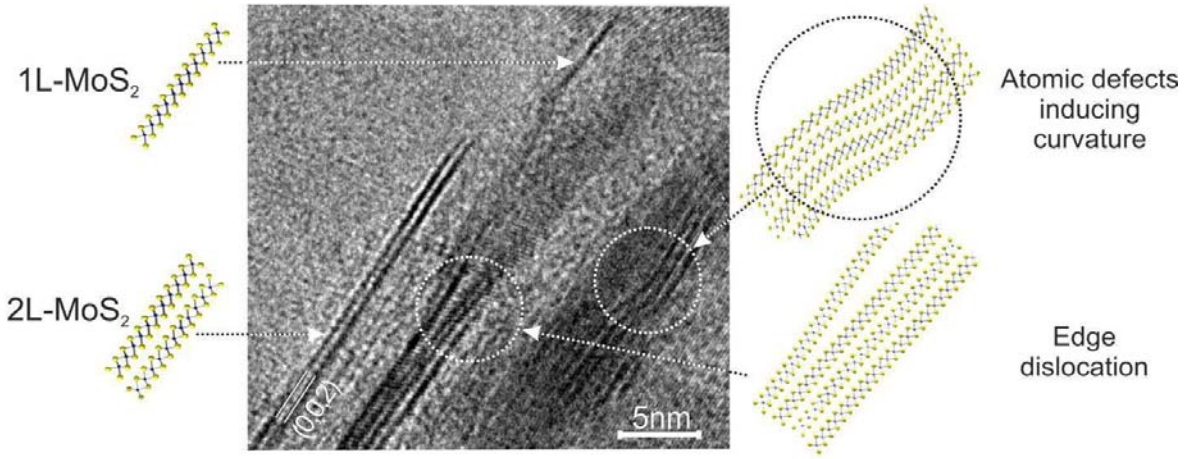

Figure 2. HRTEM image of a sonicated MoS_2 portion in IPA for 12 hours: i) monolayer-MoS_2 (1H-MoS_2 polytype) and two-layered MoS_2 slabs (2H-MoS_2 polytype), shown by the dotted arrows in the figure, are modelled on the left side; ii) atomic defects inducing plane curvature and an edge dislocation, shown by dotted circles in the figure, are modelled on the right side.

The role of the disordered atomic arrangement, causing the cracking of the basal planes with formation of additional edges, has been discussed by Xiao J. et al.,[38] while in a previous work,[35] it was shown that upon strong cavitation conditions of MoS_2 in IPA, the fragmentation of extensive layers leads to a rupture of MoSMo bonds. With the subsequent and prompt exposure of coordinatively and chemically unsaturated Mo and S species reacting with the solvent (and to a less extent with atmospheric oxygen), surface polar species (hydroxyl, alkoxide, carbonylic and carboxylate groups) are formed. We have so concluded that fragmentation and plane curvature are accompanied by extensive functionalization. It is so plausible that such functionalized surface plays a role in decorating the surface of TNTs which are covered by OH groups. Oxidation products are present also on the surface of virgin MoS_2 exposed to air as well, [39] but in a small extent for systems that can be considered with stoichiometry 1Mo:2S.

3.2 Morphology and structure of TNTs.

Titanate nanotubes were investigated by means of AFM and TEM microscopies. A single titanate nanotube of about 400 nm in length and 12 nm in diameter is AFM imaged in Figure 3a.

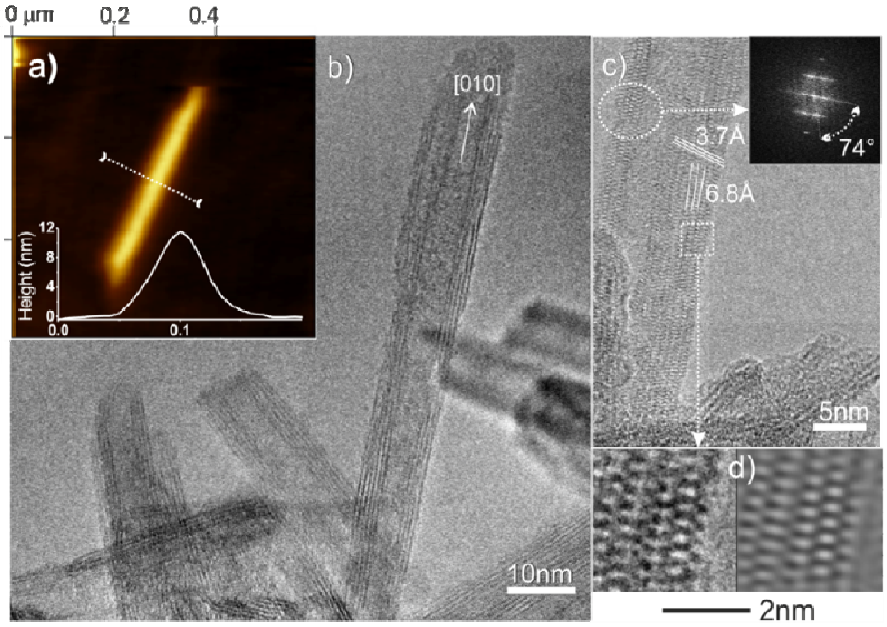

Figure 3. a) AFM image and height profile of a single TNT; b) HRTEM image of isolated TNTs; the arrow in b) indicates the [010] zone axis direction of the nanotube; c) HRTEM image of regions showing two families of planes with the corresponding FFT image in the insert; d) IFFT-unfiltered and -filtered HRTEM images of a selected area in c).

The tubular structure of titanates is TEM imaged in Figure 3b, where elongated nanostructures constituted by asymmetric walls (i.e. with different numbers of shells on both sides) are indicative of their scroll-type structure. In addition, lattice fringes ~ 0.7 nm spaced delimit an internal cavity, 3-5 nm in diameter, which is parallel to the axis of the nanotube and is accessible from the outer side. Another set of fringes ~ 0.35 nm spaced, at an angle of ~ 74° (or ~ 106°) respective to the previous one, can be observed in Figure 3c. The two observed lattice spacings can be assigned to (200) and to (003) planes, respectively, of a monoclinic $H_2Ti_3O_7$ (JCPDS Card #41-1092, a = 16.0230 Å, b= 3.7490 Å, c= 9.1910 Å, β = 101.45°). The obtained IFFT-filtered atomic resolution image (Figure 3d) can be explained with ribbons of edge-sharing TiO_6 octahedrons, joined at the corners and forming a zig-zag layered structure.[40] According to the octahedron-stepped monoclinic $H_2Ti_3O_7$, which is the widely accepted structure, the tube can be made by rolling several (100) planes around either the [010] or the [001] directions,[40] depending on the possible helicity of the nanotube as well.[40-41]

3.3. Morphology and Raman spectra of MoS_2/TNTs composite.

Due to the complex morphology of the composite, to the high MoS_2 dilution and to the low AFM resolution, MoS_2 nanosheets have not been detected by AFM after the wet impregnation step and only titanate nanotubes could be unambiguously identified. However, MoS_2 on titanate nanotubes have been TEM imaged in Figure 4(a,c,d). In Figure 4(c,d), MoS_2 made by single and few layers fragments

supported on TNTs nanotubes are evidenced. Whether these fragments are strongly adhering to the surfaces of nanotubes, cannot be inferred from HRTEM.

However as the MoS_2 is strongly functionalized with polar groups [53], the surface is fir mLy adhering to the TNTs nanotube.

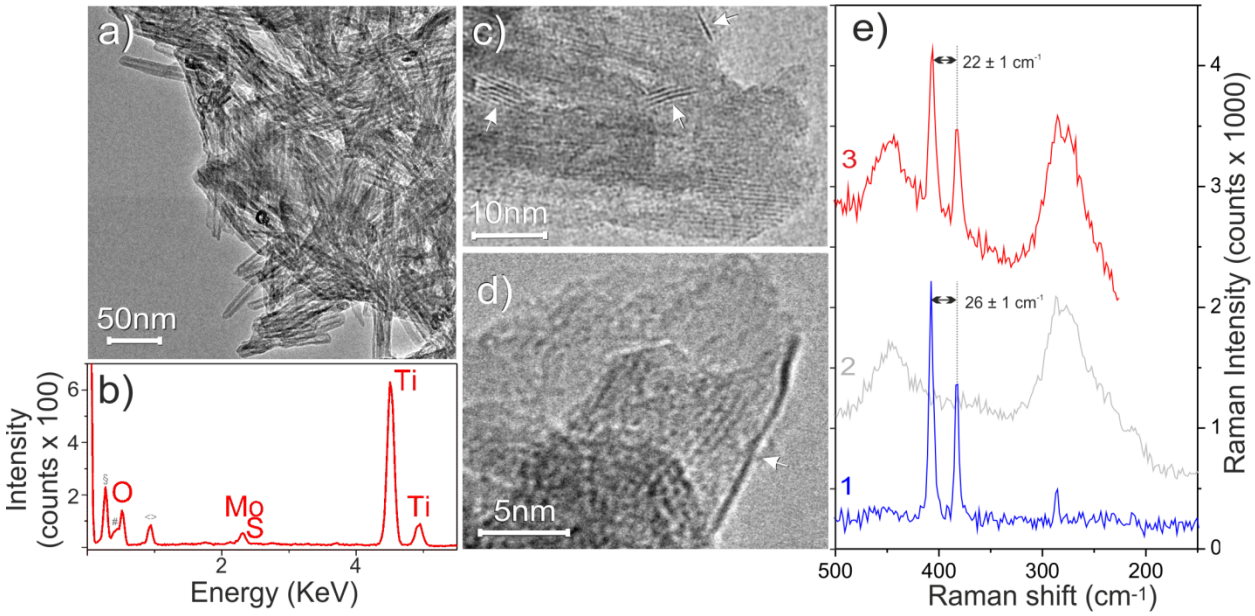

Figure 4. a) TEM image of MoS_2/TNTs composite; b) EDAX spectrum of MoS_2/TNTs composite; c), d) HRTEM images of selected regions of MoS_2/TNTs composite: the white arrows in c) and d) evidence the presence of few- and mono-layer MoS_2 slabs, respectively, adhering to the external surface of nanotubes; e) Raman spectra of the samples: (1) bulk MoS_2; (2) pure TNTs; (3) exfoliated MoS_2/TNTs composite.

As the concentration of the exfoliated MoS_2 particles is low (lower than 0.1 wt %) and the lateral sizes of the slabs are expected to be of the order of the nanotube diameter, regions showing the composite material cannot be easily recognised, although the local EDAX investigation may help in the MoS_2 identification (Figure 4b). From the low magnification TEM images, the presence of thick MoS_2 particles and of large sheets cannot be singled out (Figure 4a). Nevertheless, from the obtained HRTEM images (Figure 4c,d), few- and mono-layer MoS_2 slabs, with lateral sizes of 3-10 nm and decorating the external surface of nanotubes, appear to be isolated and well distributed. This means that during the wet impregnation phase, re-stacking phenomena of MoS_2 particles are avoided. Although the pores of the nanotubes are accessible, MoS_2 particles have not been observed inside the cavities. This means that, despite the apparent flexibility and the sufficiently small sizes of the slabs, they do not enter the nanotubes and different preparation methods, under investigation, have to be used.

In Figure 4e the Raman spectra of the MoS_2/TNTs composite (red curve) are compared with those of the two precursor materials (protonated titanate nanotubes: grey curve; and bulk MoS_2: violet curve). Raman spectrum of the bulk MoS_2 (Figure 4e, curve 1) shows two narrow peaks with maxima at 409 cm^{-1} and at 383 cm^{-1} (Δ=26 cm^{-1}), which are assigned to the A_{1g} and E^1_{2g} first order Raman active modes, respectively. The in-plane E^1_{2g} mode is generated from opposite vibrations of two S atoms with respect to

the Mo atom, while the A_{1g} mode arises from the out-of-plane vibration of only S atoms in opposite direction.[42] Other two modes are expected in this interval (E^2_{2g} and E_{1g}), but they are too low in energy and in intensity to be measured by our instrument.

Raman spectrum of the protonated titanate nanotubes (Figure 4e, curve 2) shows broad bands centred at 277 cm^{-1} and at 445 cm^{-1}. In order to assign these two bands, the variety of the crystalline order and habits of the titanate phases should be considered.[43] According to the literature, the bands at lower wavenumbers can be assigned to symmetric stretching modes of short Ti-O bonds within the layer structure (277 cm^{-1}) [44] and to the break of symmetry along the rearranged and bent TiO_6 layers (peak at 287 cm^{-1}).[45] The Raman band at 445 cm^{-1} has been ascribed to 2D lepidocrocite-type TiO_6 octahedral layers.[43] In any case, the presence of anatase and rutile, which are precursors and products of titanate decomposition, can be excluded.

Raman spectrum of the MoS_2/TNTs composite (Figure 4e, curve 3) shows fingerprints of both single phases: at 445 cm^{-1}, at 405 cm^{-1} and at 382 cm^{-1} and at 277 cm^{-1}.

The frequency difference between A_{1g} and E^1_{2g} first-order Raman active modes of MoS_2 can be considered as an indicator of the thickness of the particle.[23] Therefore on the basis of the obtained results, the frequency values of the MoS_2 film, used as reference (bulk like), closely correspond to those (narrower) reported in the literature for bulk systems,[35] whereas a stacking number of 4 ± 1 layers (Δ=23.0 ± 1.0 cm^{-1}), is obtained for the MoS_2/TNTs composite, thus confirming an effective dispersion of the molybdenum disulphide on the nanotubes. It is most noticeable that the half widths of the A_{1g} and E^1_{2g} peaks of MoS_2/TNTs composite are larger than that of the reference film and of that of bulk MoS_2, as expected for highly dispersed and supported systems.

In Scheme 1 a model of the arrangement of MoS_2 platelets on TNTs is shown, which summarizes the previously discussed TEM and Raman results. As confirmed by TEM investigations, the platelets do not insert into the cavity, but decorate the surface of TNTs.

The presence of Ti-OH groups on the surface of the nanotubes is responsible for electrostatic interactions with the oxygen-rich surface of MoS_2. In addition, the sonicated and exfoliated MoS_2 nanosheets do not restack during impregnation and, even after the removal of the solvent, they maintain the separation degree obtained during sonication (mean value of three/four layers of MoS_2), as confirmed by Raman spectrum of the MoS_2/TNTs composite and by the optical spectra on the UV-vis (*vide infra*).

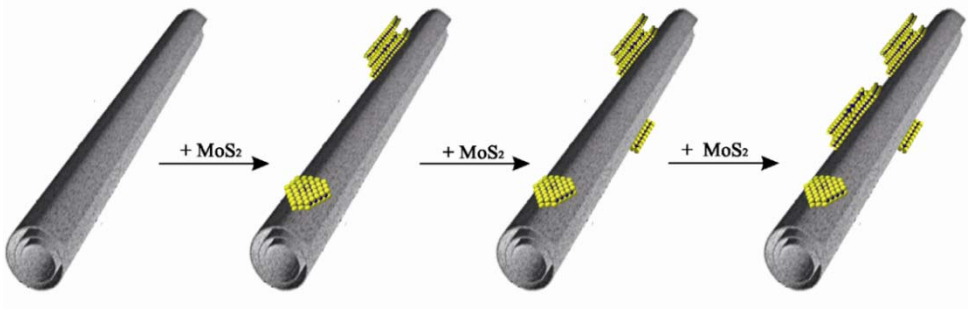

Scheme 1.

3.4. Optical properties MoS_2 particles in solution and supported on titanate nanotubes.

The absorbance spectrum of sonicated and centrifuged solution of MoS_2 is reported in Figure 5a (curve 2)**.** In the same figure the spectrum (obtained in the reflectance mode) of the most concentrated MoS_2/TNTs composite (curve 4) is reported. Curve 1 is the spectrum in the reflectance mode of pure TNTs while curve 3 is the sum of spectra 1 and 2.

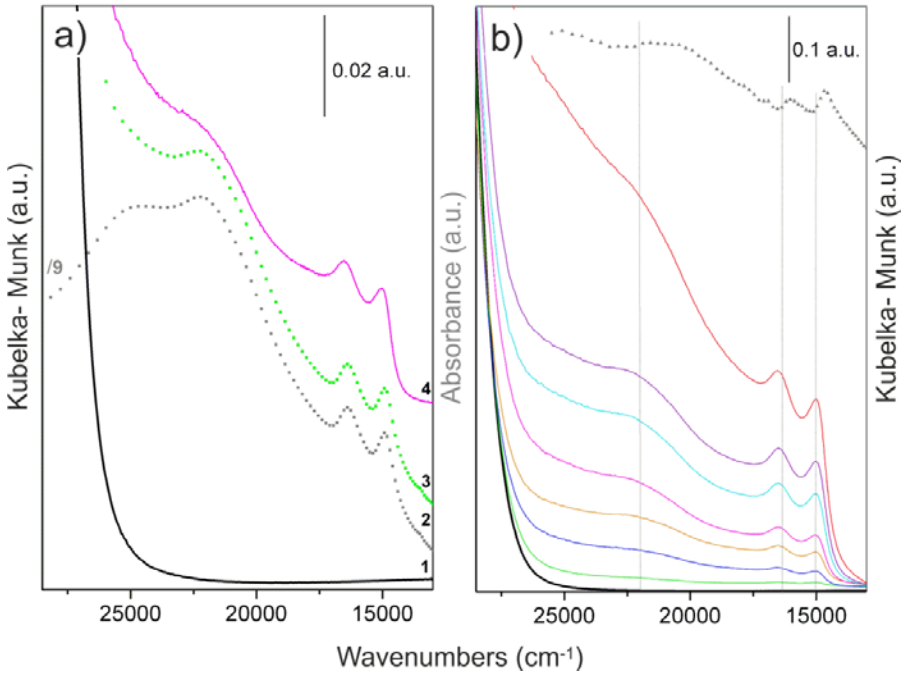

Figure 5. a) Curve 1 is the spectrum in the reflectance mode (Kubelka-Munk function) of pure TNTs. Curve 2 is the absorbance spectrum obtained in transmittance mode of MoS_2 ultracentrifuged solution: the four absorption peaks present in the spectrum of the solution correspond to four different excitonic transitions. Curve 3 is the sum of this spectrum (curve 2) with that of pure TNTs support (curve 1). Curve 4 is the experimental spectrum in the reflectance mode of the MoS_2/TNTs composite, characterized by A and B intensities, comparable to those of the calculated spectrum (curve 3). b) Absorbance spectra (Kubelka-Munk) obtained in the reflectance mode of MoS_2/TNTs composites at increasing concentrations of MoS_2 obtained by addition of increasing amounts (from 0.44 to 17.6 mL) of sonicated MoS_2 in IPA. The gray dotted curve is the spectrum obtained in the reflectance mode of bulk MoS_2 used as a reference.

In order to verify whether the optical properties of supported MoS_2 are influenced by the concentration, in Figure 5b the spectra of MoS_2/TNTs composites containing increasing concentrations of MoS_2 are illustrated.

On the basis of the literature data[46] and on our previous results,[35] it comes that the spectral features of the MoS_2 reference (gray dotted line in Figure 5b) can be assigned as follows: i) a first absorption threshold at about 700 nm (14285 cm^{-1}) due to a direct transition at the K point,[47] ii) two sharp peaks at 680 nm (14700 cm^{-1}) and at 621 nm (16100 cm^{-1}), on the high energy side of the 700nm threshold, due to A and

B excitonic transitions, respectively, whose separation energy, about 59 nm ($\Delta \sim 1400$ cm^{-1}), can be explained with spin-orbit splitting of the top of the valence band at the K point,[48] iii) a second threshold, at about 500 nm (20000 cm^{-1}), due to a direct transition from the deep in the valence band to the conduction band; iv) excitonic transitions (C and D) at 482 nm (20746 cm^{-1}) and at 399 nm (25062 cm^{-1}), respectively, also associated with the 500 nm threshold transition,[46] v) a third threshold at about 350 nm (28571 cm^{-1}) due to transitions from deep in the valence band.

In the spectrum of the solution of sonicated MoS_2, (Figure 5a, curve 2) two couples of bands are also observed at 14900 cm^{-1} and 16400 cm^{-1} (narrow, A and B excitons) and at 22270 cm^{-1} and 24810 cm^{-1} (broad and intense envelope due to C and D excitonic transitions). According to literature data, in this figure the typical features of MoS_2 nanoparticles in solutions are singled out.[49-52]

Notice that the two couples of bands are slightly shifted to higher energies to a different extent, if compared to those of the MoS_2 film.[23] More exactly, in comparison to the reference values (MoS_2 film) the energy values of A and B excitons are only slightly upward shifted, whereas larger shifts are observed for C and D excitons, according to the fact that quantum size effects are affecting C and D bands in more remarkable way.

As widely discussed in literature,[14] quantum size effects increase the band gap in nanoscale MoS_2: the smaller are the MoS_2 particles, the higher is the band gap and the associated absorption. Some authors[52] report that strong blue shifts occur in MoS_n ($n \sim 2.5$) when the lateral dimensions of the nanoparticles are reduced to < 50 nm. By comparing the spectra of the sonicated system to that of the reference film (bulk-like) we can conclude that the observed features are only slightly shifted to higher energy values with respect to the bulk. This behaviour reflects moderate quantum size effects in agreement with the presence of mono-few layers platelets ranging in the 5-10 nm interval, together with a not negligible amount of very small sized particles.[35]

Moving now to the spectrum of titanate nanotubes (Figure 5a, curve 1), an absorption edge at about 28570 cm^{-1} (350 nm), which is blue shifted with respect to that of the TiO_2 precursor (anatase and rutile), can be observed.[36] This shift to higher frequency is explained with the decreased dimensionality by moving from 3D (TiO_2 precursors) to 1D (titanate nanotube) systems.

From Figure 5a it can be seen that the sum of the spectrum obtained in solution with that of TNTs support (curve 3) is very similar to that obtained experimentally (curve 4). From this it is inferred that the supporting procedure is not substantially affecting the spectrum of MoS_2. Even the C-D bands, which are near to the adsorption edge of TNTs, are not substantially influenced, the only difference being represented by broadening as expected for supported material, where some heterogeneity is necessarily present. As the experimental spectrum (curve 4) of the low concentration composite considered in this study is substantially the sum of the spectra of the two pure components (curve 3), this means that TNTs and MoS_2 particles behave as independent entities, even if the HRTEM experiments are showing that the MoS_2 single layer nanoparticles and TNTs phases are in close contact. In turn this implies that the C-D excitonic transitions of MoS_2 particles and the charge transfer absorption of TNTs support corresponding

to the promotion of one electron from the valence to the conduction band do not influence each other. A plausible consequence is that the excitonic excitation at 22-25000 cm^{-1} (C-D bands) is not accompanied by high efficient transfer of the excited electron in MoS_2 phase to the conduction band of TNTs.

Of course this conclusion is valid only for TNTs support, which has a band gap at about 26500 cm^{-1} (~3.4 eV). It is expected that due to the lower band gap of TiO_2 (~ 3 eV), TiO_2/MoS_2 composites can behave in a different manner because the C-D bands of MoS_2 fall nearly at the TiO_2 band gap energy. Indeed this conclusion has been obtained for TiO_2/MoS_2 composites characterized by MoS_2 concentrations 2 order of magnitude larger (30-70 wt % MoS_2)[27] and hence characterized by full saturation of the optical transitions in the visible. To verify whether this promoting effect is also present on low concentrated systems like those used in this study, still characterized by intense and well defined transitions in the visible, an investigation is in progress.

The sequence of spectra reported in Figure 5b, all characterized by A-B excitonic transition not changing with the concentration, allows also to conclude that an increment of concentration is not affecting the particles dispersion. This result is the expected one when the low MoS_2 concentration and the high surface area of TNTs support are considered.

3.5. Comparison of methylene blue photodegradation activity of pure TNTs, TiO_2 (P25) and MoS_2/TNTs hybrid structures.

In Figure 6a the spectrum of ~ 1.5 monolayers of MB adsorbed on TNTs is illustrated. This spectrum is identical to the spectrum of MB adsorbed on MoS_2/TNTs. A very similar spectrum is also observed for the same dose of MB adsorbed on TiO_2 (P25) (Supporting Information, Figure S4) the only difference being represented by the lower intensity of the low frequency peak. It is known that MB in solution shows a distinct tendency to form agglomerates.[53-54] The same happens in the adsorbed state.[55] Monomeric and polymeric species are in thermodynamic equilibrium. The relative concentration of these species is mainly dictated by the monolayer and multilayer character of the adsorbed phase and by the adsorption and aggregation enthalpies. A plausible hypothesis is that MB in the first layer, where the interaction with the support is predominating, is under monomeric form. On the contrary the formation of aggregates not interacting with the surface is favoured in the second and outer layers. For a given quantity of adsorbed MB, the concentration of monomeric species, which are in direct contact with the surface, is expected to depend on the surface area of the support. The surface area of TNTs is definitely larger than that of TiO_2 (P25): so the relative concentration of monomeric species is expected to be higher, in agreement with the experimental results.

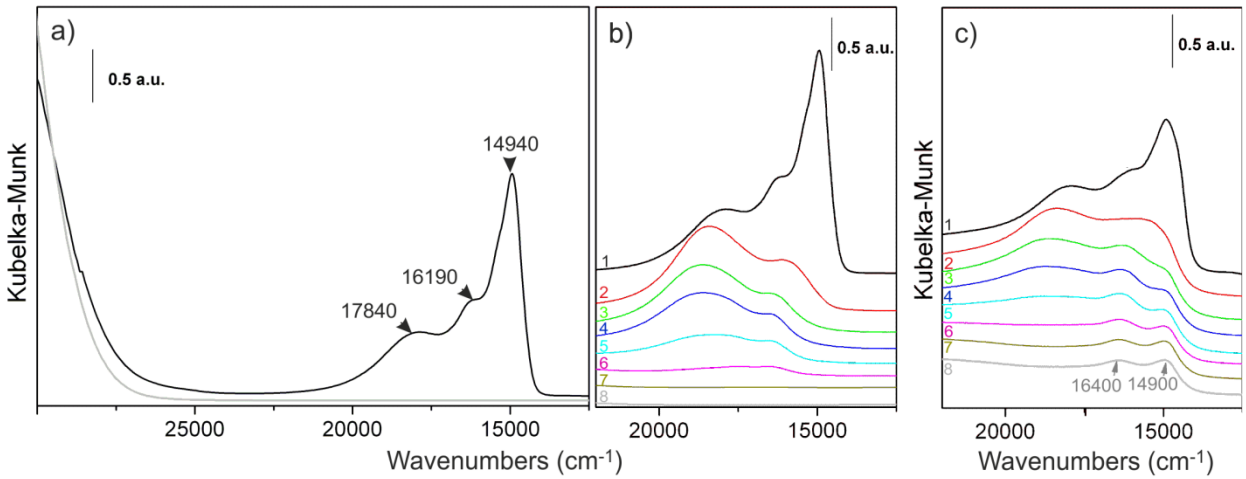

Figure 6. a) UV-vis spectrum of MB adsorbed on TNTs (black line). The three bands at 14940 cm^{-1}, 16190 cm^{-1}, 17840 cm^{-1} correspond to monomeric, dimeric and polymeric species, respectively; evolution of the MB spectra adsorbed on TNTs b) and on MoS_2/TNTs c) upon increasing the illumination time with the visible light (curve 1: 0 min, curve 2: 6 min, curve 3: 12 min, curve 4: 18 min, curve 5: 33 min, curve 6: 63 min, curve 7: 153 min, curve 8: 1053 min).

As for the polymeric species in the adsorbed state, it is known that the frequency is influenced by the interaction with the surface. Jockusch *et al* [56] have found that the frequency of aggregates interacting with dendrimeric surfaces are characterized by a frequency shifted towards higher frequency (18200 cm^{-1}) with respect to free aggregates. Furthermore aggregates standing vertically or inclined on the surface [57] absorb at slightly different frequencies.

On the basis of the abundant literature mentioned above, it is safely concluded that the bands centred at ~14940 cm^{-1}, ~16190 cm^{-1} and ~17840 cm^{-1} (Figure 6a,b) can be attributed to monomeric, dimeric and polymeric species, the monomeric species being located in the first layer and the dimeric/polymeric species most probably in the second and outer layers.

As TNTs are acidic materials, it can be asked whether protonation is occurring in the adsorbed state. This question can be answered on the basis of the spectroscopic results obtained in strongly acidic solutions[58] or adsorbed on strongly acidic zeolites,[59] which have shown that protonated species are characterized by a distinctly lower frequency (~ 13300 cm^{-1}). As this band is totally absent in the spectra of Figure 6a,b, it is concluded that the acid strength of OH groups of TNTs is not high enough to cause MB protonation and that interaction via hydrogen bonding is favoured.

The photodegradation experiments illustrated in Figure 6b,c demonstrate clearly that monomeric species are readily consumed followed by the dimeric and later on by the polymeric ones. Notice that the frequency of polymeric species increases when the monomeric species forming the first layer are consumed. This is due to the fact that the polymeric species, initially in the second and outer layers, become directly adsorbed on the surface upon consumption of the molecules of the first layer. The extinction coefficients of monomeric, dimeric and polymeric species are likely slightly different. For this

reason the use of integrated intensity of the three components of the MB spectrum as an estimate of surface MB concentration is intrinsically approximate. However, as we are only interested in the comparison between results concerning identical bands present on similar solid surfaces, this approximation is acceptable. The reasonableness of the degradation results, obtained on the basis of this assumption, has been checked by controlling the photodegradation experiments carried out in solution (Supporting Information, Figure S2). From this, no significant effects on the photodegradation of MB are observed, within the limits of experimental error.

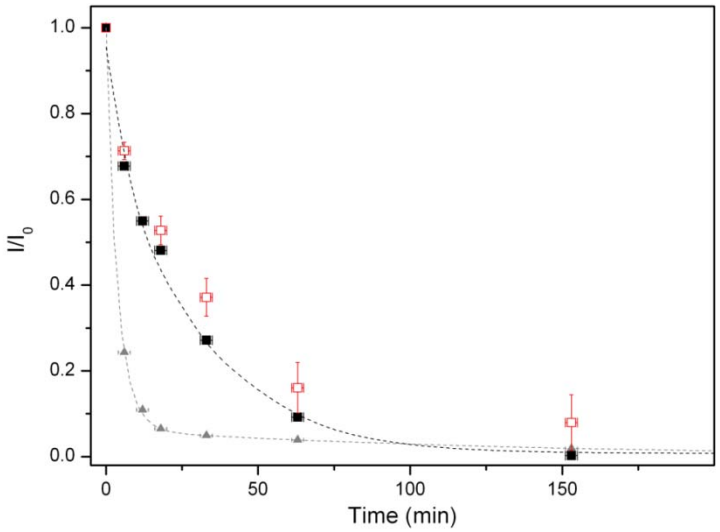

Figure 7. Evolution with illumination time of the MB concentration adsorbed on TiO_2 (P25) (triangles), on TNTs (squares) and on MoS_2/TNTs (red squares).

The photodegradation results are shown in Figure 7. It can be seen that the activity of TiO_2 (P25) is definitely larger than that of pure TNTs. The difference is so high that we are sure that the approximate character of our method is not affecting the conclusion. From this result, it can be concluded that TNTs band gap value (definitely higher than that of TiO_2) is playing the major role in determining the poorer photoactivity under visible light illumination and that the higher SSA of TNTs is not counterbalancing the previous negative effect. The surface area of TNTs (~300 m^2/g) and of P25 TiO_2 (~55 m^2/g) have not been altered by the impregnation with MoS_2 under the adopted MoS2 quantity and within the BET experimental error (±5%).

The second conclusion is that MoS_2/TNT composite substantially shows the same activity of TNTs. The data are more approximate than those obtained on TNTs because they are obtained after subtraction of the MoS_2 A-B excitonic bands, which being characterized by considerable intensity, are inducing a substantial uncertainty. From this comparison, it is inferred that, despite the favourable optical properties, in terms of frequency and intensity values, ensured by the presence in the MoS_2/TNTs system of A, B, C, D excitonic bands in the 15-25000 cm^{-1} interval, the photodegradation properties are not altered. Unlike

hypothesized for TiO_2/MoS_2 composites,[27] this can be either due to the poor match between the high frequency C-D excitonic peaks and the TNTs band gap frequency or to the high dilution, which counterbalances the positive effect of the presence of the strong C and D bands, which alter the optical properties of the composite.

It must be recalled that a positive effect has been indeed observed for TiO_2/MoS_2 composites, characterized by more than 30% [27, 25] MoS_2 concentrations, which are orders of magnitude larger than those used in this study. To solve this problem, more concentrated systems, although are not characterized by a well defined spectrum in the visible, will be prepared and an experimental study is under way.

4. Conclusions

MoS_2/TNTs hybrid composites have been obtained by wet impregnation of high surface area titanate nanotubes (TNTs) with a centrifuged solution of MoS_2 particles, formed by exfoliation/fragmentation under intense ultrasound cavitation in isopropyl alcohol (IPA). It is verified that the ultracentrifuged portion of MoS_2 in IPA is characterized by very good dispersion and that the major fraction of particles has single/few layer structure and size distribution in the 5-15 nm range.

From HRTEM images of partially exfoliated portions of IPA suspension, defective regions are clearly visible, being edge dislocations and plane curvatures a proof of the strong cavitation and the small lateral sizes of the slabs an indication of the fragmentation perpendicular to the basal planes. On the final composite, isolated and well distributed mono- and few-layers MoS_2 slabs are decorating the external surface of the nanotubes, whereas MoS_2 is not penetrating into the cavities of nanotubes. Raman spectra of the samples confirm the good dispersion of the MoS_2 slabs on the outer wall surfaces of the nanotubes.

It is shown that the method can be of general validity for the impregnation of high surface area materials with MoS_2 nanoparticles. Another advantage of the method is associated with the high volatility of IPA solvent which, being easily removed after impregnation by simple evaporation at 80°C, allows the preparation of composites at low temperature and free of carbonaceous impurities. The optical properties of MoS_2 nanoparticles measured in IPA suspension, as studied by means of UV-vis-NIR, are dominated by the strong excitonic transitions in the visible,which are only slightly shifted with respect to the bulk because of the quantum size effect. These properties are substantially maintained in the final composite after the impregnation process.

The true novelty of this paper is represented by spectroscopic measurements in the reflectance mode showing that MoS_2 concentrations less than 0.1 wt% are enough to induce strong and well defined absorption in the visible. The presence of the well defined spectrum of MoS_2 allows to verify whether the presence of these strong excitonic absorption bands (A, B, C, D) can alter the photocatalytic properties of TNTs. To this end the photodegradation experiments of methylene blue (MB) have been performed on TNTs and MoS_2/TNTs. This study has been performed by reflectance spectroscopy by measuring the decay of the spectrum of MB adsorbed on the surface of TNTs upon illumination with visible light. It is

demonstrated that the MB adsorbed in the first layer is consumed first, followed by clustered MB in the second and more external layers. It is shown that the presence of low concentrated MoS_2 nanoparticles, closely interacting with the TNTs surface and responsible of high absorbance in the visible, does not substantially alter the photocatalytic properties of TNTs (which are definitely lower than those of TiO_2 (P25) used as reference). It is inferred that the poor overlap between the high frequency C, D excitonic transitions of MoS_2 and the TNTs band gap transition is likely responsible of this result.

ASSOCIATED CONTENT

Supporting Information

Additional HRTEM images of 1L and ML- MoS_2, lattice parameters as obtained from the inverse fast Fourier transform (IFFT) images are shown. A photodegradation experiment of methylene blue on MoS_2/TNT hybrid structure has also been reported. This material is available free of charge via the Internet at http://pubs.acs.org.

AUTHOR INFORMATION

Corresponding Author

*E-mail: federico.cesano@unito.it. Fax: + 39 011 6707855. Ph: + 39 011 6707834.

Author Contributions

The manuscript was written through the contributions of all authors. All authors have given approval to the final version of the manuscript.

ACKNOWLEDGMENTS

This work was supported by MIUR (Ministero dell'Istruzione, dell'Università e della Ricerca), INSTM Consorzio and NIS (Nanostructured Interfaces and Surfaces) Inter-Departmental Centre of University of Torino.

ABBREVIATIONS

TNTs: titanate nanotubes; IPA: isopropyl alcohol; MB: methylene blue; 1H-MoS_2: molybdenum disulfide monolayer; 2H-MoS_2: bulk molybdenum disulfide; SSA: specific surface area; UV-vis-NIR spectroscopy: UV-visible near infrared spectroscopy; HRTEM: high-resolution transmission electron microscopy; AFM: atomic force microscopy; FFT: fast Fourier transform; IFFT: inverse fast Fourier transform.

References:

1. Xu, M.; Liang, T.; Shi, M.; Chen, H., Graphene-Like Two-Dimensional Materials. *Chem. Rev.* **2013**, *113*, 3766−3798.

2. Cravanzola, S.; Haznedar, G.; Scarano, D.; Zecchina, A.; Cesano, F., Carbon-Based Piezoresistive Polymer Composites: Structure and Electrical Properties. *Carbon* **2013**, *62*, 270-277.

3. Sun, Z.; Haixin Chang, H., Graphene and Graphene-Like Two-Dimensional Materials in Photodetection: Mechanisms and Methodology. *ACS Nano* **2014**, *8*, 4133-4156.

4. Li, N.; Liu, G.; Zhen, C.; Li, F.; Zhang, L.; Cheng, H.-M., Battery Performance and Photocatalytic Activity of Mesoporous Anatase Tio_2 Nanospheres/Graphene Composites by Template-Free Self Assembly. *Adv. Funct. Mater.* **2011**, *21*, 1717-1722.

5. Wang, D.; Choi, D.; Li, J.; Yang, Z.; Nie, Z.; Kou, R.; Hu, D.; Wang, C.; Saraf, L. V.; Zhang, J.; Aksay, I. A.; Liu, J., Self-Assembled Tio_2–Graphene Hybrid Nanostructures for Enhanced Li-Ion Insertion. *ACS Nano* **2009**, *3*, 907-914.

6. Cesano, F.; Bertarione, S.; Damin, A.; Agostini, G.; Usseglio, S.; Vitillo, J. G.; Lamberti, C.; Spoto, G.; Scarano, D.; Zecchina, A., Oriented Tio_2 Nanostructured Pillar Arrays: Synthesis and Characterization. *Adv. Mater.* **2008**, *20*, 3342-3348.
7. Cesano, F.; Pellerej, D.; Scarano, D.; Ricchiardi, G.; Zecchina, A., Radially Organized Pillars of Tio_2 Nanoparticles: Synthesis, Characterization and Photocatalytic Tests. *J. Photochem. Photobiol. A. Chem.* **2012**, *242*, 51-58.
8. Liang, Y.; Wang, H.; Casalongue, H. S.; Chen, Z.; Dai, H., Tio_2 Nanocrystals Grown on Graphene as Advanced Photocatalytic Hybrid Materials *Nano Res* **2010**, *3*, 701-705.
9. Williams, G.; Seger, B.; Kamat, P. V., Tio_2-Graphene Nanocomposites. Uv-Assisted Photocatalytic Reduction of Graphene Oxide. *ACS Nano* **2008**, *2*, 1487-1491.
10. Zhang, Y.; Pan, C., Tio_2/Graphene Composite from Thermal Reaction of Graphene Oxide and Its Photocatalytic Activity in Visible Light. *J. Mater. Sci.* **2011**, *46*, 2622-2626.
11. Tang, Y.-B.; Lee, C.-S.; Xu, J.; Liu, Z.-T.; Chen, Z.-H.; He, Z.; Cao, Y.-L.; Yuan, G.; Song, H.; Chen, L.; Luo, L.; Cheng, H.-M.; Zhang, W.-J.; Bello, I.; Lee, S.-T., Incorporation of Graphenes in Nanostructured Tio_2 Films Via Molecular Grafting for Dye-Sensitized Solar Cell Application. *ACS Nano* **2010**, *4*, 3482-3488.
12. Wang, X.; Zhi, L.; Mullen, K., Transparent, Conductive Graphene Electrodes for Dye-Sensitized Solar Cells. *Nano Lett.* **2008**, *8*, 323-327.
13. Yang, N.; Zhai, J.; Wang, D.; Chen, Y.; Jiang, L., Two-Dimensional Graphene Bridges Enhanced Photoinduced Charge Transport in Dye-Sensitized Solar Cells. *ACS Nano* **2010**, *4*, 887-894.
14. Hu, K. H.; Hu, X. G.; Xu, Y. F.; Pan, X. Z., The Effect of Morphology and Size on the Photocatalytic Properties of Mos_2. *React. Kinet. Mech. Catal.* **2010**, *100*, 153-163.
15. Yin, Z.; Li, H.; Li, H.; Jiang, L.; Shi, Y.; Sun, Y.; Lu, G.; Zhang, Q.; Chen, X.; Zhang, H., Single-Layer Mos_2 Phototransistors. *ACS Nano* **2012**, *6*, 74-80.
16. Stephenson, T.; Li, Z.; Olsen, B.; Mitlin, D., Lithium Ion Battery Applications of Molybdenum Disulfide (Mos_2) Nanocomposites. *Energy Environ. Sci.* **2014**, *7*, 209-231.
17. Merki, D.; Fierro, S.; Vrubel, H.; Hu, X., Amorphous Molybdenum Sulfide films as Catalysts for Electrochemical Hydrogen Production in Water. *Chem. Sci.* **2011**, *2*, 1262.
18. Rao, C. N. R.; Maitra, U.; Waghmare, U. V., Extraordinary Attributes of 2-Dimensional Mos_2 Nanosheets. *Chem. Phys. Lett.* **2014**, *609*, 172-183.
19. Raybaud, P.; Hafner, J.; Kresse, G.; Kasztelan, S.; Toulhoat, H., Ab Initio Study of the H2–H2s/Mos2 Gas–Solid Interface: The Nature of the Catalytically Active Sites. *J Catal* **2000**, *189*, 129-146.
20. Tye, C. T.; Smith, K. J., Catalytic Activity of Exfoliated Mos_2 in Hydrodesulfurization, Hydrodenitrogenation and Hydrogenation Reactions. *Top. Catal.* **2006**, *37*, 129-135.
21. Nielsen, J. H.; Bech, L.; Nielsen, K.; Tison, Y.; Jørgensen, K. P.; Bonde, J. L.; Horch, S.; Jaramillo, T. F.; Chorkendorff, I., Combined Spectroscopy and Microscopy of Supported Mos_2 Nanoparticles. *Surface Science* **2009**, *603*, 1182-1189.
22. Kibsgaard, J.; Lauritsen, J. V.; Lægsgaard, E.; Clausen, B. S.; Topsøe, H.; Besenbacher, F., Cluster-Support Interactions and Morphology of Mos_2 Nanoclusters in a Graphite-Supported Hydrotreating Model Catalyst. *JACS* **2006**, *128*, 13950-13958.
23. Cesano, F.; Bertarione, S.; Piovano, A.; Agostini, G.; Rahman, M. M.; Groppo, E.; Bonino, F.; Scarano, D.; Lamberti, C.; Bordiga, S.; Montanari, L.; Bonoldi, L.; Millini, R.; Zecchina, A., Model Oxide Supported Mos_2 Hds Catalysts: Structure and Surface Properties. *Catal. Sci. Technol.* **2011**, *1*, 123-126.
24. Chatterjee, D.; Mahata, A., Visible Light Induced Photodegradation of Organic Pollutants on Dye Adsorbed Tio_2 Surface. *J. Photochem. Photobiol. A. Chem.* **2002**, *153*, 199-204.
25. Hu, K. H.; Hu, X. G.; Xu, Y. F.; Sun, J. D., Synthesis of Nano-Mos_2/Tio_2 Composite and Its Catalytic Degradation Effect on Methyl Orange. *J. Mater. Sci.* **2010**, *45*, 2640-2648.
26. Girish, K. S.; Gomathi, D. L., Review on Modified Tio_2 Photocatalysis under Uv/Visible Light: Selected Results and Related Mechanisms on Interfacial Charge Carrier Transfer Dynamics. *J. Phys. Chem. A* **2011**, *115*, 13211-13241.
27. Zhou, W.; Yin, Z.; Du, Y.; Huang, X.; Zeng, Z.; Fan, Z.; Liu, H.; Wang, J.; Zhang, H., Synthesis of Few-Layer Mos_2 Nanosheet Coated Tio_2 Nanobelt Heterostructures for Enhanced Photocatalytic Activities. *Small* **2013**, *9*, 140-147.
28. Shanmugam, M.; Bansal, T.; Durcan, C. A.; Yu, B., Molybdenum Disulphide/Titanium Dioxide Nanocomposite-Poly 3-Hexylthiophene Bulk

Heterojunction Solar Cell. *Appl. Phys. Lett.* **2012**, *100*, 153901.
29. Thurston, T. R.; Wilcoxon, J. P., Photooxidation of Organic Chemicals Catalyzed by Nanoscale Mos_2. *J. Phys. Chem. B* **1999**, *103*, 11-17.
30. Tang, Y.; Jiang, Z.; Tay, Q.; Deng, J.; Lai, Y.; Gong, D.; Zhili, D.; Zhong, C., Visible-Light Plasmonic Photocatalyst Anchored on Titanate Nanotubes: A Novel Nanohybrid with Synergistic Effects of Adsorption and Degradation. *RSC Adv.* **2012**, *2*, 9406-9414.
31. Perera, S. D.; Mariano, R. G.; Vu, K.; Nour, N.; Seitz, O.; Chabal, Y.; Balkus, K. J., Jr., Hydrothermal Synthesis of Graphene-Tio_2 Nanotube Composites with Enhanced Photocatalytic Activity. *ACS Catal.* **2012**, *2*, 949-956.
32. Ide, Y.; Nakasato, Y.; Ogawa, M., Molecular Recognitive Photocatalysis Driven by the Selective Adsorption on Layered Titanates. *JACS* **2010**, *132*, 3601–3604.
33. Chen, Y.; Wang, L.; Lu, G. M.; Yao, X.; Gu, L., Nanoparticles Enwrapped with Nanotubes: A Unique Architecture of Cds/Titanate Nanotubes for Efficient Photocatalytic Hydrogen Production from Water. *J. Mater. Chem.* **2011**, *21*, 5134.
34. Liu, X.; Zhang, J.; Yan, R.; Zhang, Q.; Liu, X., Preparation of Graphene Nanoplatelet–Titanate Nanotube Composite and Its Advantages over the Two Single Components as Biosensor Immobilization Materials. *Biosens. Bioelectron.* **2014**, *51*, 76-81.
35. Muscuso, L.; Cravanzola, S.; Cesano, F.; Scarano, D.; Zecchina, A., Optical, Vibrational, and Structural Properties of Mos_2 Nanoparticles Obtained by Exfoliation and Fragmentation Via Ultrasound Cavitation in Isopropyl Alcohol. *J. Phys. Chem. C* **2015**, *119*, 3791–3801.
36. Cesano, F.; Bertarione, S.; Uddin, M. J.; Agostini, G.; Scarano, D.; Zecchina, A., Designing Tio_2 Based Nanostructures by Control of Surface Morphology of Pure and Silver Loaded Titanate Nanotubes. *J. Phys. Chem. C* **2010**, *114*, 169-178.
37. Cesano, F.; Rahman, M. M.; Bertarione, S.; Vitillo, J. G.; Scarano, D.; Zecchina, A., Preparation and Adsorption Properties of Activated Porous Carbons Obtained Using Volatile Zinc Templating Phases. *Carbon* **2012**, *50*, 2047-2051.
38. Xiao, J.; Choi, D.; Cosimbescu, L.; Koech, P.; Liu, J.; Lemmon, J. P., Exfoliated Mos_2 Nanocomposite as an Anode Material for Lithium Ion Batteries. *Chem. Mater.* **2010**, *22*, 4522–4524.
39. Maugè, F.; Lamotte, J.; Nesterenko, N. S.; Manoilova, O.; Tsyganenko, A. A., Ft-Ir Study of Surface Properties of Unsupported Mos_2. *Catal. Today* **2001**, *70*, 271-284.
40. Chen, Q.; Du, G. H.; Zhang, S.; Peng, L.-M., The Structure of Trititanate Nanotubes. *Acta Crystall. Sect. B* **2002**, *58*, 587-593.
41. Yoshida, K.; Miao, L.; Tanaka, N.; Tanemura, S., Direct Observation of Tio_6 Octahedron Forming Titanate Nanotube by Advanced Transmission Electron Microscopy. *Nanotech* **2009**, *20*, 405709.
42. Li, H.; Zhang, Q.; Yap, C. C. R.; Tay, B. K.; Edwin, T. H. T.; Olivier, A.; Baillargeat, D., From Bulk to Monolayer Mos_2: Evolution of Raman Scattering. *Adv. Funct. Mater.* **2012**, *22*, 1385-1390.
43. Gao, T.; Fjellvåg, H.; Norby, P., Crystal Structures of Titanate Nanotubes: A Raman Scattering Study. *Inorg Chem* **2009**, *48*, 1423-32.
44. Qian, L.; Du, Z.-L.; Yang, S.-Y.; Jin, Z.-S., Raman Study of Titania Nanotube by Soft Chemical Process. *J. Mol. Struct.* **2005**, *749*, 103-107.
45. Menzel, R.; Peiro, A. M.; Durrant, J. R.; Shaffer, M. S. P., Impact of Hydrothermal Processing Conditions on High Aspect Ratio Titanate Nanostructures. *Chem. Mater.* **2006**, *18*, 6059-6068.
46. Wilcoxon, J. P.; Newcomer, P. P.; Samara, G. A., Synthesis and Optical Properties of Mos_2 and Isomorphous Nanoclusters in the Quantum Confinement Regime. *J. Appl. Phys.* **1997**, *81*, 7934-7944.
47. Ramakrishna Matte, H. S. S.; Gomathi, A.; Manna, A. K.; Late, D. J.; Datta, R.; Pati, S. K.; Rao, C. N. R., Mos_2 and Ws_2 Analogues of Graphene. *Angew. Chem. Int. Ed.* **2010**, *49*, 4059-4062.
48. Shi, H.; Yan, R.; Bertolazzi, S.; Brivio, J.; Gao, B.; Kis, A.; Jena, D.; Xing, H. G.; Huang, L., Exciton Dynamics in Suspended Monolayer and Few -Layer Mos_2 2d Crystals. *ACS Nano* **2013**, *7*, 1072-1080.
49. Coleman, J. N.; Lotya, M.; O'Neill, A.; Bergin, S. D.; King, P. J.; Khan, U.; Young, K.; Gaucher, A.; De, S.; Smith, R. J.; Shvets, I. V.; Arora, S. K.; Stanton, G.; Kim, H.-Y.; Lee, K.; Kim, G. T.; Duesberg, G. S.; Hallam, T.; Boland, J. J.; Wang, J. J.; Donegan, J. F.; Grunlan, J. C.; Moriarty, G.; Shmeliov, A.; Nicholls, R. J.; Perkins, J. M.; Grieveson, E. M.; Theuwissen, K.; McComb, D. W.; Nellist, P. D.; Nicolosi, V., Two-Dimensional Nanosheets Produced by Liquid Exfoliation of Layered Materials. *Science* **2011**, *331*, 568-571.
50. Quinn, M. D. J.; Ho, N. H.; Notley, S. M., Aqueous Dispersions of Exfoliated Molybdenum Dysulphide for Use in Visible-Light Photocatalysis. *ACS Appl. Mater. Interf.* **2013**, *5*, 12751.

51. Wang, K.; Wang, J.; Fan, J.; Lotya, M.; O'Neill, A.; Fox, D.; Feng, Y.; Zhang, X.; Jiang, B.; Zhao, Q.; Zhang, H.; Coleman, J. N.; Zhang, L.; Blau, W. J., Ultrafast Saturable Absorption of Two-Dimensional Mos_2 Nanosheets. *ACS Nano* **2013**, *7*, 9260-9267.
52. Wang, Y.; Ou, J. Z.; Balendhran, S.; Chrimes, A. F.; Mortazavi, M.; Yao, D. D.; Field, M. R.; Latham, K.; Bansal, V.; Friend, J. R.; Zhuiykov, S.; Medhekar, N. V.; Strano, M. S.; Kalantar-zadeh, K., Electrochemical Control of Photoluminescence in Two-Dimensional Mos_2 Nanoflakes. *ACS Nano* **2013**, *7*, 10083.
53. Florence, N.; Naorem, H., Dimerization of Methylene Blue in Aqueous and Mixed Aqueous Organic Solvent: A Spectroscopic Study. *J. Mol. Liq.* **2014**, *198*, 255-258.
54. Patil, K.; Pawar, R.; Talap, P., Self-Aggregation of Methylene Blue in Aqueous Medium and Aqueous Solutions of Bu_4nbr and Urea. *Phys Chem Chem Phys* **2000**, 4313-4317.
55. Kobayashi, H.; Sasaki, M.; Ohsawa, N.; Yasuda, K.; Kotani, M., Fluorescence and Its Density-Dependent Quenching of a Sub-Monolayer Film of Methylene Blue Prepared by Dip Coating. *J. Phys. Chem. C* **2007**, *111*, 268-271.
56. Jockusch, S.; Turro, N. J.; Tomalia, D. A., Aggregation of Methylene Blue Adsorbed on Starburst Dendrimers. *Macromolecules* **1995**, *28*, 7416-7418.
57. Fujita, K.; Taniguchi, K.; Ohno, H., Dynamic Analysis of Aggregation of Methylene Blue with Polarized Optical Waveguide Spectroscopy. *Talanta* **2005**, *65*, 1066-1070.
58. Seger, B.; Vinodgopal, K.; Kamat, P. V., Proton Activity in Nafion Films: Probing Exchangeable Protons with Methylene Blue. *Langmuir* **2007**, *23*, 5471-5476.
59. Zanjanchi, M. A.; Sohrabnezhad, S., Evaluation of Methylene Blue Incorporated in Zeolite for Construction of an Optical Humidity Sensor. *Sens. Actuat. B-Chem.* **2005**, *105*, 502-507.

MoS_2 Nanoparticles Decorating Titanate-Nanotube Surface: Combined Microscopy, Spectroscopy and Catalytic Studies

Sara Cravanzola[1], Lucia Muscuso[1], Federico Cesano[1]*, Giovanni Agostini[2], Alessandro Damin[1], Domenica Scarano[1] and Adriano Zecchina[1]

[1]*Department of Chemistry, NIS (Nanostructured Interfaces and Surfaces) Interdepartmental Centre and INSTM Centro di Riferimento, University of Torino, Via P. Giuria, 7, 10125 Torino (Italy).*

[2]Current address: giovanni.agostini@esrf.fr

Supporting Information

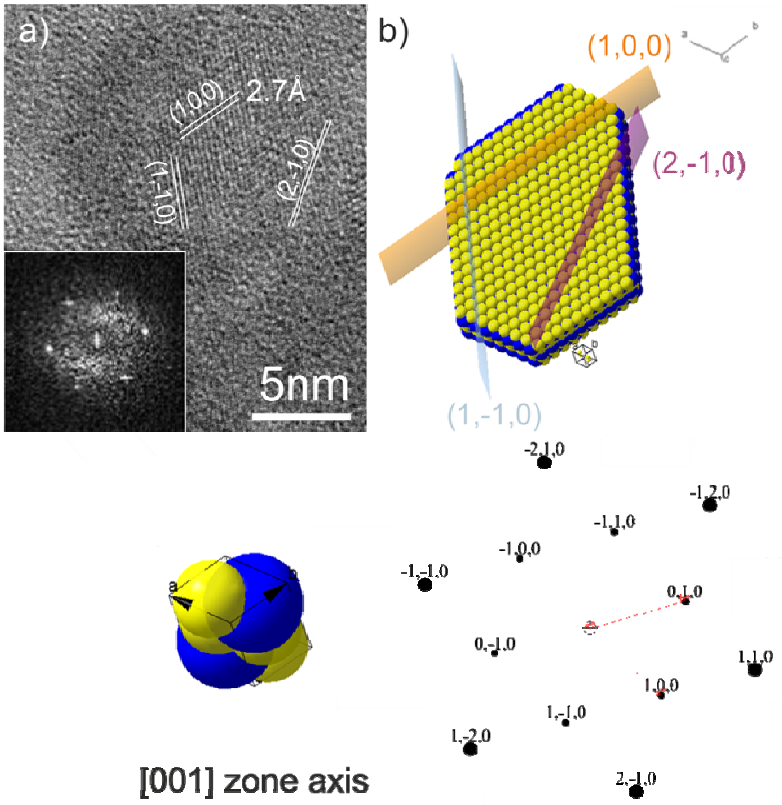

Figure S 1. a) HRTEM image of a ML-MoS_2 slab, b) model of the selected particle in a); simulated electron diffraction pattern from the [001] zone axis (bottom panel). In the insert of a) the experimental electron diffraction pattern is shown.

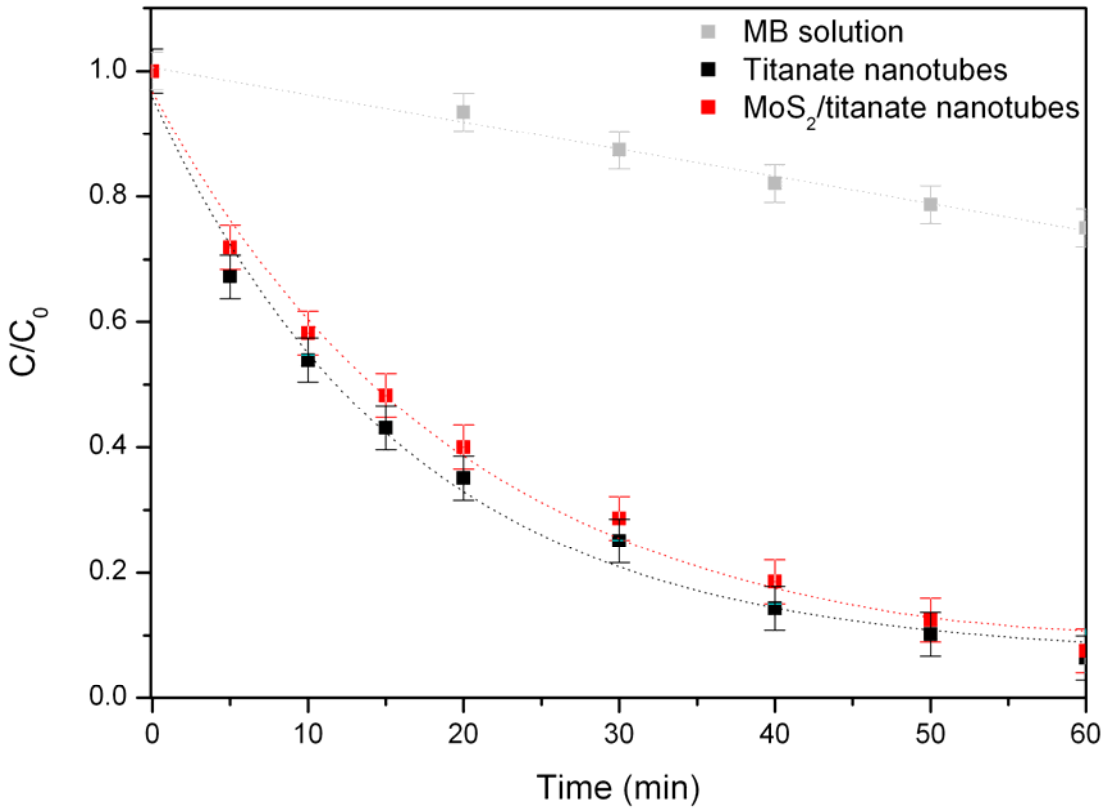

Figure S 2. C/C_0 MB band evolution in the liquid phase along the illumination time for TNTs (black squares) and for MoS_2/TNTs (red squares). The C/C_0 MB band evolution for the pure MB solutions exposed to the light (no photocatalyst added) is shown for comparison (grey squares).

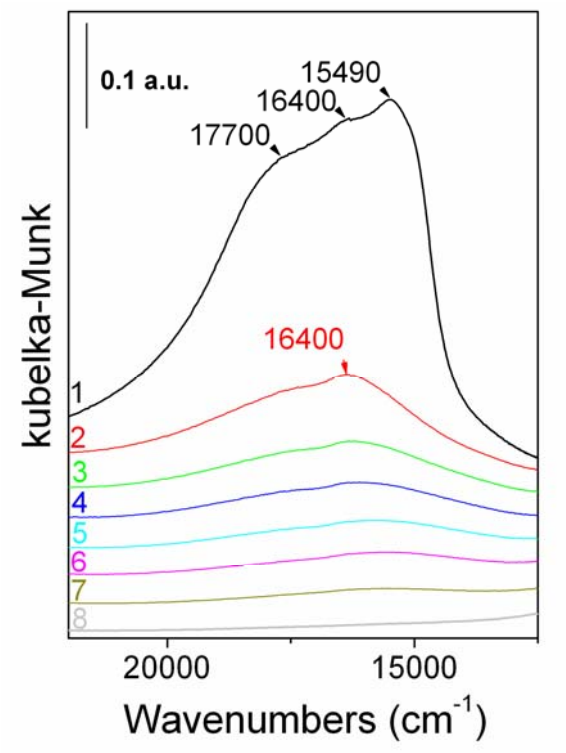

Figure S 3. UV-Vis spectrum of MB adsorbed on P25 (black line). The three bands at ~15500 cm^{-1}, ~16400 cm^{-1}, ~17700 cm^{-1} correspond to monomeric, dimeric and polymeric species, respectively; evolution of the MB spectra adsorbed on P25 upon the illumination time (curve 1: 0 min, curve 2: 6 min, curve 3: 12 min, curve 4: 18 min, curve 5: 33 min, curve 6: 63 min, curve 7: 153 min, curve 8: 1053 min).